Optimizing Hand/Eye Configuration for Visual-Servo Systems

Rajeev Sharma **Seth Hutchinson**
The Beckman Institute, University of Illinois at Urbana-Champaign
405 N. Mathews Avenue, Urbana, IL 61801

Abstract

We derived a quantitative measure of the ability of a camera setup to observe the changes in image features due to relative motion [10]. This measure of motion perceptibility *has many applications in evaluating a robot hand/eye setup with respect to the ease of achieving vision-based control, and steering away from singular configurations. Motion perceptibility can be combined with the traditional notion of manipulability, into a composite perceptibility/manipulability measure. In this paper we demonstrate how this composite measure may be applied to a number of different problems involving relative hand/eye positioning and control. These problems include optimal camera placement, active camera trajectory planning, robot trajectory planning, and feature selection for visual servo control. We consider the general formulation of each of these problems, and several others, in terms of the motion perceptibility/manipulability measure and illustrate the solution for particular hand/eye configurations.*

1 Introduction

In recent years, there has been a growing interest in visual servo control of robotic manipulators [1]. A typical visual servo setup includes a robot and either a fixed supervisory camera (*e.g.* [4, 11]) or a camera mounted directly on the robot (*e.g.* [7, 13]). In either case, the image observed by the camera changes due to motion of the robot. Visual servo controllers compute a control input for the robot based on the relationship of differential changes in the image to differential changes in the configuration of the robot. This relationship is captured by the image Jacobian [2, 13].

Most visual servo controllers are designed so that the error signal is defined directly in terms of some set of image features (image-based control), rather than in terms of the absolute position of the robot (position-based control) [1]. Therefore, how the image features change with the motion of the robot has a direct effect on the performance of a visual servo control system. For example, if a large motion of the robot produces very little change in the image features, then it may be difficult to use the differential change in the measured features to derive the control input. Hence there is a need for some quantitative measure of the ability to observe changes in the image features with respect to the motion of the robot.

Similar concern with respect to the differential change in the end-effector position (and orientation) relative to change in the joint configuration resulted in the definition of the term *manipulability* [14] or *dexterity* [3]. These measures, which depend on the particular robot mechanism and its posture, capture a sense of how far the robot is from a singular configuration. For robot control, singular configurations are undesirable since at those configurations the ability to move along one or more dimensions of the task space is lost. The manipulability measures are thus used in designing robot mechanisms or in determining the optimal configuration with respect to robot control.

In this paper, we are concerned with the notion of *motion perceptibility*, whose purpose is to quantify the ability of the computer vision system to perceive certain robot motions. Analogous to the motion of a robot end-effector, the "motion" of the image features may be near singular configurations with respect to the object that the camera is observing. The motion perceptibility measure gives a sense of how far the camera/object configuration is from the visual singularities. Motion perceptibility may be combined in a intuitive manner with the classical manipulability measure to give a composite perceptibility/manipulability measure. The composite perceptibility/manipulability can be used as a performance measure for driving several applications in visual servo control. We explore several of these applications with the help of examples involving different hand/eye configurations.

2 Motion Perceptibility

Let $\mathbf{J}_v$ be the Jacobian matrix that relates differential changes in the visual features observed by a camera to differential changes in the position of the robot

$$\dot{\mathbf{v}} = \mathbf{J}_v \dot{\mathbf{r}} \tag{1}$$

where $\mathbf{v}$ is a vector of observed image features, and $\mathbf{r}$ denotes a configuration of the robot tool.

In [10] we introduced a measure of *motion perceptibility*, that quantifies the magnitude of changes to image features that result from motion of the tool. We denote this measure by w_v, defined by

$$w_v = \sqrt{\det(\mathbf{J}_v^T \mathbf{J}_v)} \tag{2}$$

In general there are three cases to consider, depending on the dimensions of $\mathbf{J}_v$. In this paper, we consider only the case in which $\mathbf{J}_v \in \mathbf{R}^{n \times n}$. In this case we have

$$w_v = |\det(\mathbf{J}_v)|. \tag{3}$$

There are other quantitative methods that have been used to evaluate the perceptibility of motion. For example, in the context of feature selection, Feddema [2] has used the condition number for the image Jacobian, given by $\|\mathbf{J}_v\| \|\mathbf{J}_v{}^{-1}\|$. Nelson and Khosla have proposed resolvability [6], which is similar to motion perceptibility that we have introduced in [10]. Designing a visual servo control system requires concern for both motion perceptibility, and for how effectively the robot can manipulate objects in certain configurations. The concept of manipulability has been formalized by Yoshikawa [14], and is defined by

$$w_r = \sqrt{\det(\mathbf{J}_r \mathbf{J}_r^T)} \tag{4}$$

where $\mathbf{J}_r \in \mathbf{R}^{n \times n}$ is the manipulator Jacobian matrix given by $\dot{\mathbf{r}} = \mathbf{J}_r \dot{\mathbf{q}}$, (in which $\dot{\mathbf{q}}$ is the vector of robot joint velocities and $\dot{\mathbf{r}}$ is the vector of the end effector velocities).

It is straight forward to combine motion perceptibility with manipulability by noting that

$$\dot{\mathbf{v}} = \mathbf{J}_v \mathbf{J}_r \dot{\mathbf{q}} = \mathbf{J}_c \dot{\mathbf{q}}. \tag{5}$$

IEEE International Conference
on Robotics and Automation
0-7803-1965-6/95 $4.00 ©1995 IEEE

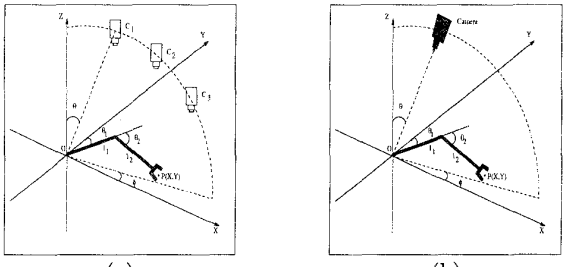

(a) (b)

Figure 1: Two hand/eye configurations with a movable camera and a 2-dof planar robot. In (a) the orientation of the camera is fixed, parallel to the world z-axis, while in (b) the camera always points toward the origin of the world coordinate frame.

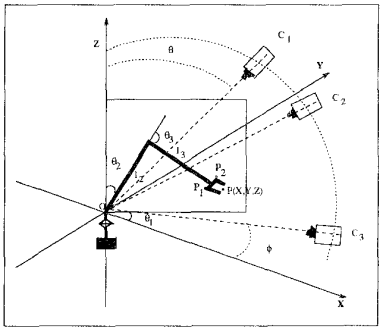

Figure 2: The schematic of the second hand/eye configuration with a movable camera and a 3-dof puma-type robot.

Here, the composite Jacobian $\mathbf{J}_c$ relates differential changes in configuration of the robot to differential changes in the observed visual features. We define a composite measure of perceptibility/manipulability as,

$$w = \sqrt{\det(\mathbf{J}_c^T \mathbf{J}_c)}. \tag{6}$$

Note that this applies only to a non-redundant robot; the case of redundant robot has been treated in [9]. w measures the perceptibility of the joint velocity rather than the perceptibility of motion of the robot tool. In this case, if a particular joint motion cannot be perceived, there are two possible causes: the vision system cannot observe the corresponding motion of the tool (a singularity in the image Jacobian), or the robot is in a configuration in which certain tool velocities are not possible (a singularity in the manipulator Jacobian). For the case of redundant robots, $w = 0$, since $\text{rank}(\mathbf{J}_c^T \mathbf{J}_c) \leq m < n$ and $\mathbf{J}_c^T \mathbf{J}_c \in \mathbf{R}^{n \times n}$. In general, $w \neq w_v w_r$, except in the special non-redundant case when $n = m = k$. The equality $(w = w_v w_r)$, is achieved in this case because both $\mathbf{J}_r$ and $\mathbf{J}_v$ are square matrices [9].

3 Visual Servo Control Setups

In this section, we introduce the visual servo control setups that we will use to study the application of the motion perceptibility, w_v, and the composite perceptibility/manipulability, w.

A 2-DOF Planar Arm. First we consider two examples, each involving a two-link planar arm and a moveable camera. In each case, we define the task space to be the set of positions that the robot tool can reach. We parameterize the task space by (x, y), the position in the plane of the robot's tool center, P. The configuration space of the robot can be parameterized by the two joint angles, (θ_1, θ_2). For the first example, we fix the orientation of the camera such that its optical axis is parallel to the z-axis of the world coordinate frame. This setup is illustrated in Figure 1a. For the second example, we constrain the camera to always point toward the origin of the world coordinate frame, as illustrated in Figure 1b. In each case, we parameterize the camera configuration by the spherical coordinates (R, θ, ϕ).

For visual servo control of the 2-DOF robot, two image parameters are sufficient. Here, we use the image coordinates (u, v) of the point P. We assume that the end effector is always in the field of view of the camera, so that the image of P can be extracted. For this case, we have the following:

$$\mathbf{J}_r = \begin{bmatrix} l_1 \cos\theta_1 + l_2 \cos(\theta_1 + \theta_2) & l_2 \cos(\theta_1 + \theta_2) \\ -l_1 \sin\theta_1 - l_2 \sin(\theta_1 + \theta_2) & -l_2 \sin(\theta_1 + \theta_2) \end{bmatrix}$$

$$w_r = |det\mathbf{J}_r| = l_1 l_2 |\sin\theta_2|$$

$$\mathbf{J}_v = \begin{bmatrix} \frac{-f}{R\cos\theta} & 0 \\ 0 & \frac{-f}{R\cos\theta} \end{bmatrix}, \quad w_v = |det\mathbf{J}_v| = \frac{f^2}{R^2 \cos^2\theta}. \tag{7}$$

Since $\mathbf{J}_v$ and $\mathbf{J}_r$ are square matrices, we have

$$w = \sqrt{\det(\mathbf{J}_c^T \mathbf{J}_c)} = w_v w_r = \frac{f^2 l_1 l_2 |\sin\theta_2|}{R^2 \cos^2\theta}. \tag{8}$$

A 3-DOF PUMA-type Arm. Here we consider a Puma-type robot with three degrees of freedom, and a moveable camera. We define the task space to be the set of positions that the robot tool can reach, parameterized by (x, y, z). The configuration space of the robot can be parameterized by the three joint angles, $(\theta_1, \theta_2, \theta_3)$. We constrain the camera to always point toward the origin of the world coordinate frame, as illustrated in Figure 2, and we parameterize the camera configuration by the spherical coordinates (R, θ, ϕ).

To achieve the necessary servo control, we track three image features. Here we use the feature vector $[u_1, v_1, u_2]^T$, where u_i, v_i are the image plane coordinates of a point P_i on the robot end effector (note that we do not use v_2 in this example). The points P_1 and P_2 are illustrated in Figure 2. The calculation of $\mathbf{J}_v$ and $\mathbf{J}_r$ is straightforward, and are omitted here. As above, because both $\mathbf{J}_v$ and $\mathbf{J}_r$ are square, $w = w_v w_r$.

4 Applications

4.1 Optimal Camera Positioning

Here we will address the problem of optimal camera placement for a fixed camera system that is used to control a robot performing some predetermined motion, *e.g.* a robot grasping an object.

We briefly formalize the problem of optimal camera placement with respect to our composite measure of perceptibility/manipulability w. With respect to perceptibility, we do not address issues related to other camera placement criteria, *e.g.* occlusion, field of view, depth of field, focus, *etc.* These issues have been addressed in [8, 12]. In fact, the methods presented in [12] produce a set of constraints on camera position and orientation that could be used as additional constraints in the optimization process discussed here.

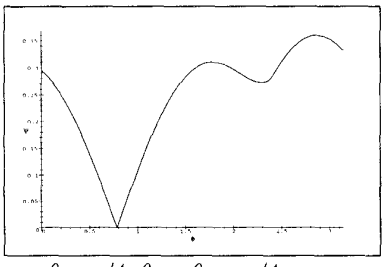

$\theta = \pi/4$; $\theta_1 = \theta_2 = \pi/4$
$\theta_3(\tau) = 2\pi\tau$, for $\tau = 0$ to $\tau = 1$

Figure 3: Variation of the performance ψ with the camera parameter, ϕ for optimal camera positioning for a given robot trajectory (see text).

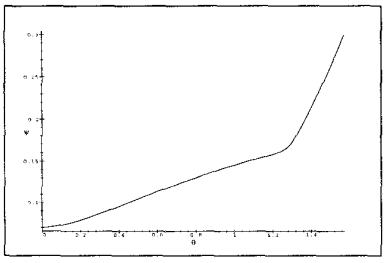

$\phi = \pi/6$; $\theta_1 = \theta_2 = \pi/4$
$\theta_3(\tau) = 2\pi\tau$, for $\tau = 0$ to $\tau = 1$

Figure 4: Variation of the performance ψ with the camera parameter, θ for optimal camera positioning for a given robot trajectory (see text).

In order to perform the optimization, we posit the following performance functional:

$$\psi(\mathbf{q}_c) = \int w(\mathbf{r}, \mathbf{q}_c)dt \tag{9}$$

where $\mathbf{q}_c$ is a vector of camera parameters that determines the camera position and orientation, $\mathbf{r}(t)$ is the parameterized trajectory followed by the robot end-effector, and the integral is taken over the duration of a given trajectory. With this formulation, the problem of optimal camera placement reduces to finding $\mathbf{q}_c^*$ such that

$$\psi(\mathbf{q}_c^*) = \max_{\mathbf{q}_c \in \mathcal{C}_c} \int w(\mathbf{r}, \mathbf{q}_c)dt. \tag{10}$$

When other viewpoint constraints are taken into account, such as those given in [12], $\mathcal{C}_c$ would be restricted to the set of valid camera configurations.

Consider the problem of optimal camera placement for the case of 3-dof puma-type robot setup of section 3, for a given trajectory of the robot. Figure 3 shows the variation of the performance ψ with respect to the camera parameter, ϕ. The performance is obtained by integrating the composite perceptibility/manipulability measure over the entire robot trajectory. A simple trajectory of the robot is chosen, which essentially moves the end-effector in a circular path by moving only one joint at a time. The optimal position of the camera correspond to the maxima in the plotted curves. Figure 4 shows the corresponding plots when only the camera parameter θ is allowed to vary for positioning the camera. The integration was carried out numerically using the XMAPLE software.

Consider the trajectory of the 2-dof planar robot setup in Figure 1b, obtained by keeping θ_1 fixed and varying θ_2 as a function of the parameter τ, as follows: $\theta_2 = sin(\pi\tau/2) + cos(\pi\tau/2)$. Figure 5 plots this trajectory and the variation of the performance measure ψ (obtained by integrating w over the entire trajectory) as a variation of the camera parameter ϕ, giving the optimal camera position as illustrated.

4.2 Active Camera Trajectory Planning

In this section, we consider the case when the camera is *actively* moved during the motion of the robot. Camera trajectory planning has many applications, particularly for repetitive operation of a robot in a very cluttered workspace, for example, in welding or painting in a car's interior. The implementation could involve two cooperating eye-in-hand robot systems, with one robot monitoring the operation of the robot performing a given task. This is an example of

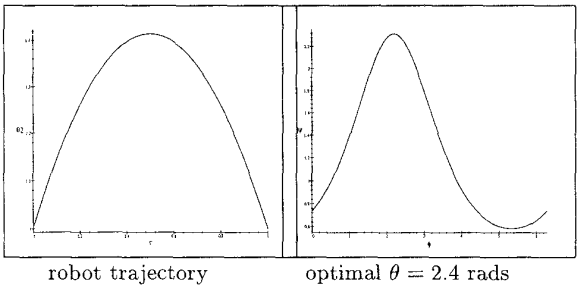

robot trajectory optimal $\theta = 2.4$ rads

Figure 5: Finding the optimal camera position for a given robot trajectory for the 2-dof planar robot.

active vision, which holds great promise in improving visual servoing as well other vision-based operation [8].

To optimize the camera trajectory we must find a camera trajectory, $\mathbf{q}_c^*(t)$, such that

$$\psi(\mathbf{q}_c^*(\cdot)) = \max_{\mathbf{q}_c(\cdot)} \int w(\mathbf{r}, \mathbf{q}_c)dt. \tag{11}$$

This formulation represents a very difficult optimization problem. Furthermore, to ensure a physically realizable camera trajectory, kinematic constraints might have to be considered as well. In general, this class of problems can only be solved by placing strict limitations on the class of trajectories that are permitted for the active camera.

For the following computed examples, to simplify the optimization procedure, we use a greedy algorithm that determines the locally best move of the camera at each time interval. In particular, if the robot and camera are in configurations $\mathbf{q}$ and $\mathbf{q}_c$, respectively, we select $\delta\mathbf{q}_c^*$ such that

$$w(\mathbf{q}, \mathbf{q}_c + \delta\mathbf{q}_c^*) = \max_{\delta\mathbf{q}_c} w(\mathbf{q}, \mathbf{q}_c + \delta\mathbf{q}_c). \tag{12}$$

At each stage, the set of possible choices for $\delta\mathbf{q}_c$ is restricted to reflect the set of reachable positions when kinematic constraints are incorporated in the camera motion. The optimization is carried out numerically using the XMAPLE software.

Consider the hand/eye setup of Figure 1b, where the camera is allowed to move only along a circle, defined by fixing θ and varying ϕ. Figure 6 shows the result of the active camera planning for two different robot trajectories with the

restriction that at each step (unit of time) the movement of the camera is bounded (0.5 radians). The starting position of the camera in both the cases is $\phi = \pi/4$. The resulting active camera trajectories can be further smoothed to incorporate kinematic constraints of the active camera mechanism. The two robot trajectories are plotted parametrically and the resulting active camera trajectories are shown that optimize the composite perceptibility/manipulability measure under the given motion constraints (Figure 6).

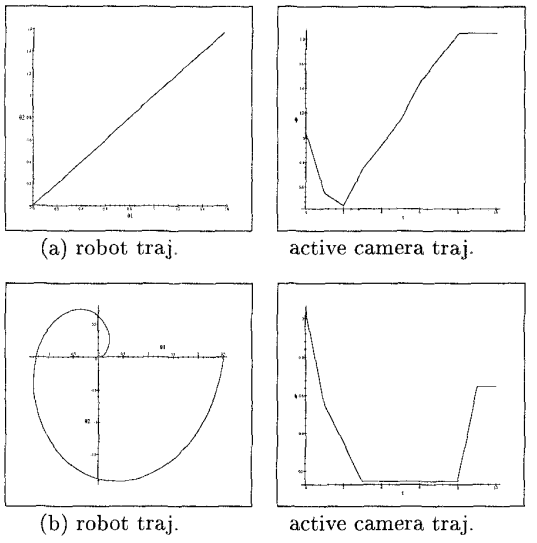

(a) robot traj. active camera traj.

(b) robot traj. active camera traj.

Figure 6: The result of active camera trajectory planning for optimizing the composite perceptibility/manipulability under given constraints, for two different trajectories of the 2-dof planar robot.

4.3 Robot Trajectory Planning

Here we show how the composite measure can be used to plan robot trajectories that avoid both kinematic and visual singularities. Here, the motion planning problem is to find a path from the initial to the final robot configuration, while at every stage maintaining the maximum value of the *composite perceptibility/manipulability measure*.

Again, to simplify the optimization procedure, we use a greedy algorithm that determines the locally best move of the robot at each time interval. In particular, if the robot and camera are in configurations $\mathbf{q}$ and $\mathbf{q}_c$, respectively, we select $\delta\mathbf{q}^*$ such that

$$w(\mathbf{q} + \delta\mathbf{q}^*, \mathbf{q}_c) = \max_{\delta\mathbf{q}} w(\mathbf{q} + \delta\mathbf{q}, \mathbf{q}_c). \quad (13)$$

At each stage, the set of possible choices for $\delta\mathbf{q}$ is restricted to reflect the set of reachable positions when kinematic constraints are incorporated in the robot motion. The optimization is carried out numerically using the XMAPLE software.

To illustrate this without describing a complete motion planner, we consider the following situation for the 2-dof planar robot. Suppose that the position of the camera in the setup of Figure 1b is fixed, and that a task of the robot is defined in terms of just the movement of the first joint θ_1. This means that the position of the second joint θ_2 can be arbitrarily changed without affecting the task. This is clearly not a realistic scenario. However, it is very similar to planning motions with a redundant robot, in which any joint velocities that lie in the null space of the manipulator Jacobian have a negligible effect on task performance. Figure 7 shows the trajectories of the second joint that would optimize w under a joint velocity bound that limits the motion of the joint to at most 0.5 radians for each unit interval. The result shows that the second joint moves to a "good" position and then remains stationary for the remaining trajectory of the first joint. The plots are for two different camera positions.

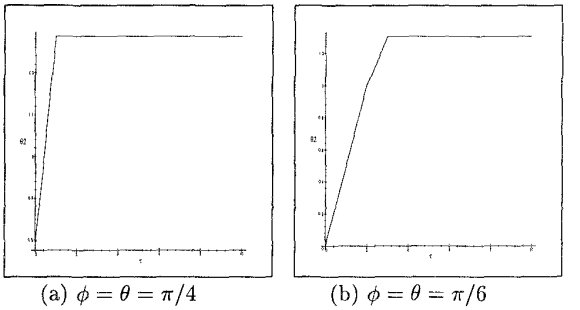

(a) $\phi = \theta = \pi/4$ (b) $\phi = \theta = \pi/6$

Figure 7: The trajectory of the "redundant" joint θ_2 to optimize the composite perceptibility/manipulability measure for the task described in text.

4.4 Simultaneous Camera/Robot Trajectory Planning

In this section we consider the *simultaneous* optimization of the robot and camera trajectories with respect to the composite perceptibility/manipulability measure. To simplify the optimization procedure, we use a greedy algorithm that determines the locally best move of both the robot and the camera at each time interval. In particular, if the robot and camera are in configurations $\mathbf{q}$ and $\mathbf{q}_c$, respectively, we select $\delta\mathbf{q}_c^*$ and $\delta\mathbf{q}^*$ such that

$$w(\mathbf{q} + \delta\mathbf{q}^*, \mathbf{q}_c + \delta\mathbf{q}_c^*) = \max_{\delta\mathbf{q}, \delta\mathbf{q}_c} w(\mathbf{q} + \delta\mathbf{q}, \mathbf{q}_c + \delta\mathbf{q}_c). \quad (14)$$

Kinematic and dynamic constraints are incorporated into the set of possible choices for $\delta\mathbf{q}$ and $\delta\mathbf{q}_c$ at each stage. A weighting factor could be used to determine the relative importance of optimizing w versus the cost of achieving the desired joint positions in terms of time or the total joint motion. The issue is basically efficiency in the robot trajectory planning versus the ease of achieving the visual servo control.

We consider again a 2-dof planar robot. We restrict the allowable camera and robot motions such that only the camera ϕ and robot joint θ_2 are allowed to change. For a simple linear trajectory of θ_1, Figure 8(a) shows the optimal trajectories for θ_2 and the camera parameter ϕ. The maximum rate of change for both θ_2 and ϕ was set to be 0.5 radians per unit time. Figure 8(b) shows the results for a more complicated trajectory of θ_1.

4.5 Feature Selection

One means of improving visual servoing is to select the right set of features from the many possible image features. In [2] for example, a method of feature selection was proposed that weighs several different criteria including photometric ones. Here we show how the measure of motion perceptibility can be factored into the feature selection process. The goal would be to select those features that will not get into "singular" configurations, in which the change in the features becomes small or even zero with robot motion.

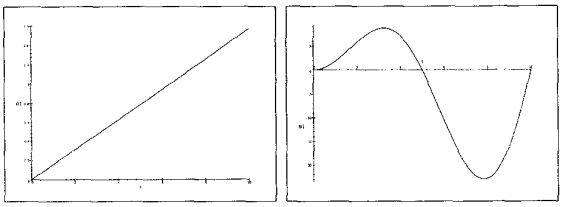

given robot motion, $\theta_1(t)$

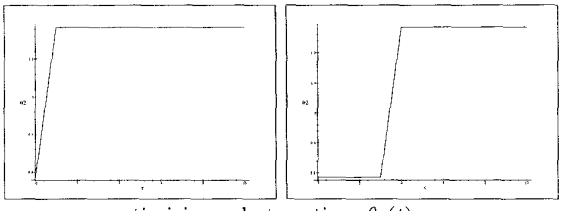

optimizing robot motion, $\theta_2(t)$

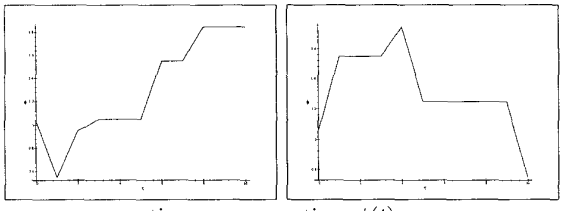

active camera motion, $\phi(t)$

Figure 8: Results of simultaneous joint (θ_2) and camera (ϕ) trajectory for optimizing the composite perceptibility/manipulability measure for the given joint trajectory (θ_1).

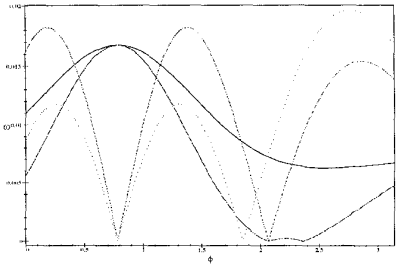

Figure 9: Composite perceptibility/manipulability as function of θ for 4 different subsets of the features.

In terms of the image jacobian, each row corresponds to one image feature, relating that feature to the differential changes in task space parameters. Thus, in terms of the motion perceptibility, one could keep a redundant image jacobian and use a subset of the rows to compute the motion perceptibility, thus maximizing its value. In general, given k features and the task of controlling m degrees of freedom, this simple approach would involve $k!/(k-m)!$ determinant computations. However some way of tracking the best candidate features could reduce the computation time. We do not consider such a scheme here. Instead we study an example of the feature selection problem for the 3-dof hand/eye setup.

Figure 9 shows the values of the composite perceptibility/manipulability plotted against a variation of the camera position parameter while using the four different subsets of three features from a candidate set of four features. One possible strategy would be to pick at one time the particular subset that gives the highest value of the motion perceptibility. This would involve switching from one subset to another at the cross-over points of the curves in Figure 9. In this example, four such "switches" would be necessary. For a given servoing task one could *a priori* divide the operating range of a camera/robot system into fixed partitions for using a particular subset of features for optimal performance in the visual servo control. Of course this analysis would also be coupled with the *geometric* consideration for determining when a feature is not occluded, and other *photometric* considerations [8]. For example, the lighting could determine which features are easiest to track.

4.6 Motion along Critical Directions

The motion perceptibility measure, w_v, described above is a single scalar quantity that is designed to give a quantitative assessment of the *overall* perceptibility of robot motions. If motion in any direction is not observable, then $w_v = 0$ (in this case $\mathbf{J}_v$ is singular). In many tasks, it is not important that the vision system be able to observe every direction of motion with high precision. Consider, for example, the peg-in-hole task illustrated in Figure 10. A simple strategy is to align the peg with the hole, push the peg into the hole. To execute this strategy, it is important that the vision system be able to observe motion in directions parallel to the surface of the block, but it is much less critical that the vision system be able to precisely observe motions in the direction perpendicular to this surface. The motion perceptibility, w_v, is not sufficient to capture such distinctions.

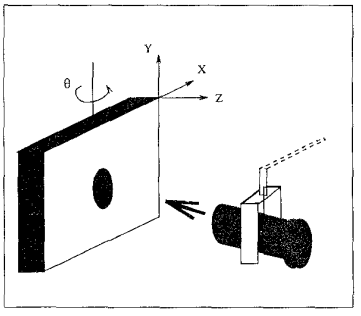

Figure 10: Example peg-in-hole task.

We can use the singular value decomposition, $\mathbf{J}_v = \mathbf{U}\Sigma\mathbf{V}$, to assess the perceptibility of motions in particular directions. Specifically, we can determine the magnitude of the visual feature velocity for a particular motion $\dot{\mathbf{r}}$ as follows.

$$\dot{\mathbf{v}} = \mathbf{J}_v\dot{\mathbf{r}} \tag{15}$$

$$= \mathbf{U}\Sigma[\mathbf{v}_1\ \mathbf{v}_2\ \ldots\ \mathbf{v}_m]^T\dot{\mathbf{r}} \tag{16}$$

$$= \mathbf{U}[\sigma_1\mathbf{v}_1\ \ \sigma_2\mathbf{v}_2\ \ \ldots\ \ \sigma_m\mathbf{v}_m]^T\dot{\mathbf{r}} \tag{17}$$

$$= \mathbf{U}\begin{bmatrix} \sigma_1\mathbf{v}_1\cdot\dot{\mathbf{r}} \\ \sigma_2\mathbf{v}_2\cdot\dot{\mathbf{r}} \\ \vdots \\ \sigma_m\mathbf{v}_m\cdot\dot{\mathbf{r}} \end{bmatrix} \tag{18}$$

Since $\mathbf{U}$ is an orthogonal matrix,

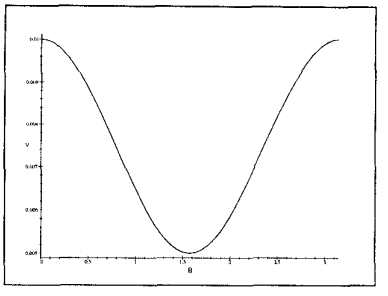

Figure 11: Plot of the modified motion perceptibility measure *vs.* viewing angle (θ).

$$\|\dot{\mathbf{v}}\| = \|[\sigma_1 \mathbf{v}_1 \cdot \dot{\mathbf{r}} \quad \ldots \quad \sigma_m \mathbf{v}_m \cdot \dot{\mathbf{r}}]^T\| \quad (19)$$

$$= ((\sigma_1 \mathbf{v}_1 \cdot \dot{\mathbf{r}})^2 + \ldots (\sigma_m \mathbf{v}_m \cdot \dot{\mathbf{r}})^2)^{1/2}. \quad (20)$$

By choosing $\dot{\mathbf{r}}$ as a weighting vector that expresses the relative importance of the perceptibility of the different directions of robot motion, we can use (20) to evaluate the camera configuration. For the example peg-in-hole task, assuming that the hole is a perfect circle, we would let $\dot{\mathbf{r}} = [0.5\ 0.5\ 0]^T$, specified in the local frame of the hole. The maximum for (20) will be achieved when $\mathbf{v}_1$ and $\mathbf{v}_2$ form a basis for the local x-y plane for the hole, and when σ_1 and σ_2 are maximized. The value for σ_3 is irrelevant, since, as described above, for this task it is not important to observe motion perpendicular to the plane containing the hole. Figure 11 shows the value of (20) as a function of θ, the orientation of the block (about it's own y-axis). As can be seen in the figure, maxima are achieved when the face of the block is parallel to the camera image plane, which matches our intuition.

5 Discussion and Conclusions

Motion perceptibility represents a single scalar measure, corresponding to the volume of the motion perceptibility ellipsoid at a particular configuration. Other scalar measures could have been used as well, for example, the ratio of the minimum diameter to the maximum diameter of the motion perceptibility ellipsoid. In the related context of manipulation, [3] gives a very good discussion for the physical meaning and shortcomings of the various dexterity measures. These dexterity measures are analogous to the motion perceptibility measure presented here.

Motion perceptibility is a local property of the relative hand/eye configurations. If a single camera is to be used for multiple tasks, for example, exploring [12] and task monitoring [5], then global optimization problems analogous to the ones posed in Section 4 would need to be solved. Such optimizations may be quite difficult to perform. Thus, one avenue for future research is to derive approximate techniques that give the most importance to the critical parameters in determining the camera position at a given time.

Despite these limitations, our measure of motion perceptibility captures a very basic property of relative camera position in a hand/eye setup. It has an intuitive meaning and provides a formal basis for positioning a camera relative to a robot for controlling an active camera, visual servo control, or trajectory planning. We have shown several example scenarios that illustrate the utility of this measure. We have shown how motion perceptibility can be combined with the manipulability measure given in [14], and explored several applications in which this composite measure can be used to optimize performance of a hand/eye system.

References

[1] P. I. Corke. Visual Control of Robot Manipulators—A Review. In K. Hashimoto, editor, *Visual Servoing*, pages 1–32. World Scientific, 1993.

[2] J. T. Feddema, C. S. George Lee, and O. R. Mitchell. Weighted Selection of Image Features for Resolved Rate Visual Feedback Control. *IEEE Transactions on Robotics and Automation*, 7:31–47, 1991.

[3] J-O. Kim and P. K. Khosla. Dexterity Measures for Design and Control of Manipulators. In *Proc. IEEE/RSJ Int. Workshop on Intelligent Robots and Systems*, pages 758–763, 1991.

[4] A. J. Koivo and N. Houshangi. Real-Time Vision Feedback for Servoing Robotic Manipulator with Self-Tuning Controller. *IEEE Transactions on Systems, Man, and Cybernetics*, 21:134–142, 1991.

[5] C. Laugier, A. Ijel, and J. Troccaz. Combining Vision-Based Information and Partial Geometric Models in Automatic Grasping. In *Proc. IEEE International Conference on Robotics and Automation*, pages 676–682, 1990.

[6] B. Nelson and P. K. Khosla. Integrating Sensor Placement and Visual Tracking Strategies. In *Proc. IEEE International Conference on Robotics and Automation*, pages 1351–1356, 1994.

[7] N. P. Papanikolopoulos, P. K. Khosla, and T. Kanade. Visual Tracking of a Moving Target by a Camera Mounted on a Robot: A Combination of Vision and Control. *IEEE Transactions on Robotics and Automation*, 9(1):14–35, 1993.

[8] R. Sharma. Active Vision for Visual Servoing: A Review. In *IEEE Workshop on Visual Servoing: Achievements, Applications and Open Problems*, May 1994.

[9] R. Sharma and S. Hutchinson. Motion perceptibility and its application to active vision-based servo control. Technical Report UIUC-BI-AI-RCV-94-05, The Beckman Institute, University of Illinois, 1994.

[10] R. Sharma and S. Hutchinson. On the Observability of Robot Motion Under Active Camera Control. In *Proc. IEEE International Conference on Robotics and Automation*, pages 162–167, May 1994.

[11] S. B. Skaar, W. H. Brockman, and R. Hanson. Camera-Space Manipulation. *International Journal of Robotics Research*, 6(4):20–32, 1987.

[12] K. Tarabanis and R. Y. Tsai. Sensor Planning for Robotic Vision: A Review. In O. Khatib, J. J. Craig, and T. Lozano-Pérez, editors, *Robotics Review 2*. MIT Press, Cambridge, MA, 1992.

[13] L. E. Weiss, A. C. Sanderson, and C. P. Neuman. Dynamic Sensor-Based Control of Robots with Visual Feedback. *IEEE Journal of Robotics and Automation*, 3:404–417, 1987.

[14] T. Yoshikawa. Analysis and Control of Robot Manipulators with Redundancy. In *Robotics Research: The First Int. Symposium*, pages 735–747. MIT Press, 1983.